Detection of Marsquake Nests in InSight Data

Raphael F Garcia, Iona Clemente, Mélanie Drilleau, Alexander Stott, Ludovic Margerin, Philippe Lognonné, Mark Panning, Bruce Banerdt

JGR Planets

RESEARCH ARTICLE

10.1029/2024JE008782

Detection of Marsquake Nests in InSight Data

Raphael F. Garcia[1], Iona Clemente[1], Mélanie Drilleau[1], Alexander Stott[1], Ludovic Margerin[2], Philippe Lognonné[3], Mark Panning[4], and Bruce Banerdt[4]

[1]Institut Supérieur de l'Aéronautique et de l'Espace (ISAE-SUPAERO), Université de Toulouse, Toulouse, France, [2]Institut de Recherche en Astrophysique et Planétologie, Université de Toulouse, CNRS, Toulouse, France, [3]Université Paris Cité, Institut de Physique du Globe de Paris, CNRS, Paris, France, [4]Jet Propulsion Laboratory, California Institute of Technology, Pasadena, CA, USA

Key Points:

- A methodology for detection and validation of quake doublet events in Mars seismic data is presented
- Three events of Very high Frequency type (S0334b, S0334c and S0343a) are validated as quakes from the same nest
- Different seismic sources (quakes and impacts) generate Very high Frequency event type

Supporting Information:

Supporting Information may be found in the online version of this article.

Correspondence to:

R. F. Garcia,
raphael.garcia@isae.fr

Citation:

Garcia, R. F., Clemente, I., Drilleau, M., Stott, A., Margerin, L., Lognonné, P., et al. (2025). Detection of marsquake nests in InSight data. *Journal of Geophysical Research: Planets*, *130*, e2024JE008782. https://doi.org/10.1029/2024JE008782

Received 14 OCT 2024
Accepted 6 JUL 2025

Author Contributions:

Conceptualization: Raphael F. Garcia
Data curation: Iona Clemente, Mélanie Drilleau
Formal analysis: Raphael F. Garcia
Funding acquisition: Raphael F. Garcia
Investigation: Iona Clemente, Alexander Stott
Methodology: Raphael F. Garcia, Iona Clemente
Project administration: Raphael F. Garcia, Philippe Lognonné, Mark Panning, Bruce Banerdt
Resources: Raphael F. Garcia, Mélanie Drilleau, Ludovic Margerin, Philippe Lognonné, Mark Panning
Software: Raphael F. Garcia, Iona Clemente, Mélanie Drilleau
Supervision: Raphael F. Garcia, Mélanie Drilleau

Abstract The seismometer of the InSight NASA discovery mission recorded more than 1,300 seismic events on Mars, grouped into different families according to their frequency content. Here, we present a method to detect quake nests based on time domain correlation of long-duration waveforms (520 s). Event doublet candidates are first detected on the 2.4 Hz local resonance, and then validated by simultaneous detections on different components and different frequency bands. We provide a detailed analysis of the impact of noise on these detections. Our method revealed a triplet of very high frequency events (S0334b/S0334c/S0343a). These observations demonstrate that quake nests do occur on Mars, validating an active seismic area at 26° epicentral distance, which is interpreted as Cerberus Fossae, and that both impacts and quakes generate the very high frequency-type seismic events. These repeating waveforms could be used to test noise removal methods applied to InSight seismic data.

Plain Language Summary Seismic events located on the same fault with the same rupture characteristics generate identical ground displacements at a seismic station over the whole duration of the record. These couples of seismic events repeating at different times are called quake doublets. Such doublets have already been observed on the Earth and on the Moon. We demonstrate that a triplet of identical quakes were recorded by SEIS (Seismic Experiment for Interior Structure) instrument on Mars surface. This information is important because such repeating events usually occur in active seismic areas and cannot be signals from meteor impacts. In addition, these records can be used as a test case for methods intending to remove noise sources from SEIS data because noise conditions of the records are different but seismic vibrations are identical.

1. Introduction

Over its 4 years of operation, SEIS (Seismic Experiment for Interior Structure), the seismometer of the NASA Discovery InSight (Interior Exploration using Seismic Investigations, Geodesy and Heat Transport) mission (Banerdt et al., 2020; Lognonné et al., 2019), detected more than 1,300 seismic events (InSight Marsquake Service, 2023). These events are classified into two main families (Giardini et al., 2020): low-frequency and high-frequency for events showing their dominant energy below and above 1 Hz, respectively. The two categories include different event types. The high-frequency family consists of three different event types: 2.4 Hz type events which only excite the 2.4 Hz local resonance, High-Frequency (HF) type events which excite the 2.4 Hz mode and frequencies up to 6 Hz and Very high Frequency (VF) type events which shows energy up to 10 Hz with larger energy on the horizontal components compared to the vertical component at frequencies larger than 5 Hz, probably due to site effect at InSight location (Carrasco et al., 2023; Hobiger et al., 2021). The low-frequency family comprises of low-frequency (LF) type and broadband (BB) type events. Contrary to BB events, the LF events do not excite the 2.4 Hz local resonance mode. The classification of these event families, largely based on the dominant frequency content of the signal, by Mars Quake Service (MQS) is presented in detail in Clinton et al. (2021). However, Stott et al. (2023) have demonstrated that some HF events also show energy below 1 Hz, as well as some LF events also show energy above 1 Hz.

Most of the High Frequency events would not have been detected without the trained eyes of the MQS frontline team because they have a low signal-to-noise ratio with values rarely exceeding 10. Because their back-azimuths are difficult to determine (Clinton et al., 2021), and have been investigated by only a single study (Stähler et al., 2022), the high-frequency events are not precisely localized, which raises questions about their origin.

Validation: Raphael F. Garcia, Alexander Stott, Ludovic Margerin
Visualization: Raphael F. Garcia, Iona Clemente
Writing – original draft: Raphael F. Garcia, Iona Clemente, Mélanie Drilleau, Alexander Stott
Writing – review & editing: Raphael F. Garcia, Alexander Stott, Ludovic Margerin, Philippe Lognonné

Without knowing their location, it is difficult to associate them to a particular tectonic feature like low-frequency events (Jacob et al., 2022; Perrin et al., 2022), or to check for impact craters thanks to orbital imaging (Garcia et al., 2022; Posiolova et al., 2022). In particular, it has been recently proposed that all VF type events are generated by impacts (Zenhäusern et al., 2024).

Repeating quake waveforms have been observed on the Earth and the Moon (Lammlein, 1977; Poupinet et al., 1984; Uchida & Bürgmann, 2019). Two different seismic records that present a good correlation over long-duration records (500 s), including the seismic wave coda, in highly scattering media are usually interpreted as seismic events occurring on the same fault with a similar, or opposite, quake mechanism (Frohlich & Nakamura, 2009; Nakamura, 1978; Weber et al., 2009). The main reason for this is that the scattered seismic wave field quickly loses its correlation properties at the receiver if the source is moved more than a quarter of the dominant wavelength (Margerin, 2013; Snieder, 2006). Using an S wave velocity of 2.4 km/s in the upper crust from recent crustal models of Mars (Drilleau et al., 2023) and a minimum frequency of 2.4 Hz, this scale length is estimated to be less than 250 m. Such events with highly correlated records over long durations are called doublets when associated in pairs, or multiplets when more than 2 events are detected. These events usually originate in seismic or volcanic active areas (Uchida & Bürgmann, 2019). The detection of seismic doublets on Mars is thus critical for two main reasons: (a) to demonstrate that these seismic events are quakes and not meteoroid impacts (Garcia et al., 2022), and so probe the question of the distribution of seismicity on Mars, and (b) to provide examples of identical quake waveforms recorded under different noise conditions which can be used to test noise removal methods.

In this study, after a short description of the data set, we present our method of doublet detection and validation tests. We then present the doublets detected in the InSight seismic data by our algorithm, and infer their respective polarities when possible. Eventually, we discuss the various implications of the presence of these repeating events and the new questions raised by our results.

2. Data

The ground velocity measurements (InSight Mars SEIS Data Service, 2019) used in this study were acquired by the Very Broad Band sensors (VBB) of the InSight mission. The raw data in counts are the three components of different sensor axes labeled U, V, and W. The sampling rate is 20 sps. Glitches (transient one-sided pulses) and tick noise (a constant electromagnetic cross-talk from a temperature measurement repeating every second) artifacts are first removed using the methods described in Scholz et al. (2020) and Compaire et al. (2021). Then, the instrument responses of the U, V, and W components are removed to convert the data into ground velocity and then rotated to the ZNE (vertical, North and East) geographical reference frame. The list of seismic events is extracted from version 14 of the Mars Quake Service (MQS) catalog (InSight Marsquake Service, 2023), where all detected events are classified into different types of events depending on the frequency content of the dominant energy (Clinton et al., 2021). We consider here all the categories of events showing significant energy above 1 Hz: 2.4 Hz, HF, VF and BB events. LF events are not used because they do not show an excitation of 2.4 Hz local resonance (Compaire et al., 2021; Hobiger et al., 2021) which is used by our detection method.

3. Detection of Quake Nests and Validation Methods

3.1. Quake Nests Detection Method

Quake doublets are usually detected by cross-correlating the signals of two different seismic events recorded at the same station over the duration of the seismic ground movements (Lammlein, 1977; Poupinet et al., 1984). Because the different event types considered (2.4 Hz, HF, VF and BB) share in common the 2.4 Hz local resonance (Compaire et al., 2021; Hobiger et al., 2021), we first band pass filter all the event records in the 2–3 Hz frequency range to make them comparable with each other. To minimize both the effect of large-amplitude artifacts (glitch, donks…) and the dependence of our results to the variations of the coda energy, only the phase information is kept by normalizing the filtered signals to 1 bit (+1 or −1). To avoid random high correlation coefficient values due to noise signals, we use a signal duration of 520 s, starting 20 s before the Pg-arrival time provided by MQS (or the event start time when the pick information is not available) and ending 500 s after. This duration is shorter than the average event duration (890 s) but long enough to include most of the P and S codas of most events (Menina et al., 2021, 2023; van Driel et al., 2021). The window duration is kept constant because the statistics of the maximum value of the correlation function is strongly dependent on this duration, shorter

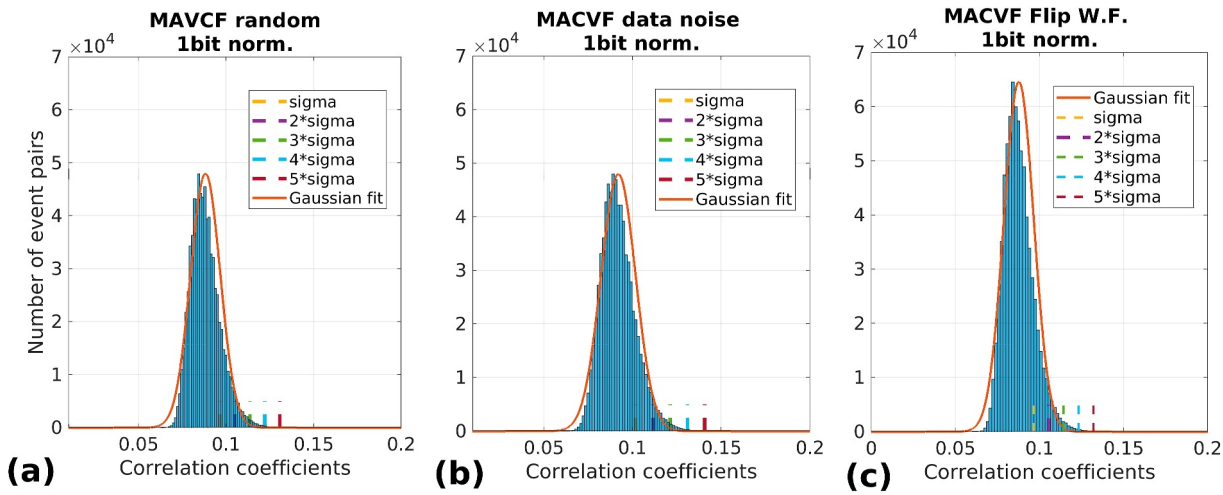

Figure 1. Distribution of Maximum Absolute Values of the Correlation Functions (MAVCF) for (a) 520 s of white noise filtered in the 2–2.8 Hz bandwidth with an order 3 band-pass filter in order to reproduce the spectral shape of 2.4 Hz resonance, (b) for 520 s of vertical component data before the seismic events filtered in the 2–3 Hz bandwidth, and (c) for 520 s of event waveform with 520 s of time reversed waveform of another event. The red line shows a Gaussian fit to the distribution. The 1 to 5 standard deviation (sigma) values are displayed with dashed lines.

windows generating higher correlation values than longer windows. Then, for each pair of the 1,226 total events considered, the cross-correlation functions are computed, and the Maximum Absolute Value of the Correlation Functions (MAVCF) between the two records is calculated along with the corresponding relative time shift between the records at this maximum value.

As a relatively large correlation coefficient is expected for a true event doublet, only pairs of events with a correlation coefficient larger than a given threshold are considered to be a potential doublet (Uchida & Bürgmann, 2019). To define this threshold value, we performed the analysis described above on three different data sets: synthetic records of white noise samples, SEIS records of 520 s of noise recorded just before the seismic events, and SEIS records of the seismic events for which one of the two tested records is time reversed before the computation of the correlation function. The histograms of the MAVCF are presented in Figure 1 for the ∼1.5 million event couples. Most of the MAVCF values from these tests are smaller than 0.17, only the last test yields 2 values between 0.17 and 0.195, and none above 0.2. As a consequence, we chose 0.17 as a detection threshold for the MAVCF parameter in this first selection step.

Figures 2a–2c shows the MAVCF statistics calculated for the InSight event data using each of the three components in the 2–3 Hz frequency bandwidth. 5, 1 and 3 event couples are detected on the vertical, North and East components, respectively. The InSight seismic events are labeled by mission Sol of occurrence (a Sol is a Martian day, whose duration is 24h 40 min) and sublabeled alphabetically for sols with more than one event (Banerdt et al., 2020). One doublet (S0343a/S0334b) is detected on all three components, and two other doublets (S0334b/S0334c and S1008a/S1073d) are identified on both vertical and East components.

We repeated the analysis in the 4–6 Hz and 6–8 Hz bandwidths. No doublets are identified on the vertical component, but several clear detections, well above the threshold, appear in the North and East components due to the local site effect (Carrasco et al., 2023) which amplifies the horizontal components relative to the vertical one above 4 Hz. In the 6–8 Hz bandwidth (Figures 2g–2i), the same 3 doublets (S0343a/S0334b, S0343a/S0334c and S0334b/S0334c) are detected on both North and East components with MAVCF values that are clearly outliers, in the 0.2–0.35 range, compared to the distribution based on noise (Figure 1).

3.2. Doublet Candidate Selection Criteria

To validate that an event couple is a doublet, the MAVCF and the time shifts are also computed without considering the 1 bit data normalization, but saturating the data above 4 sigma variation to cancel the high amplitude artifacts. The doublet candidate is validated if it meets all the following conditions:

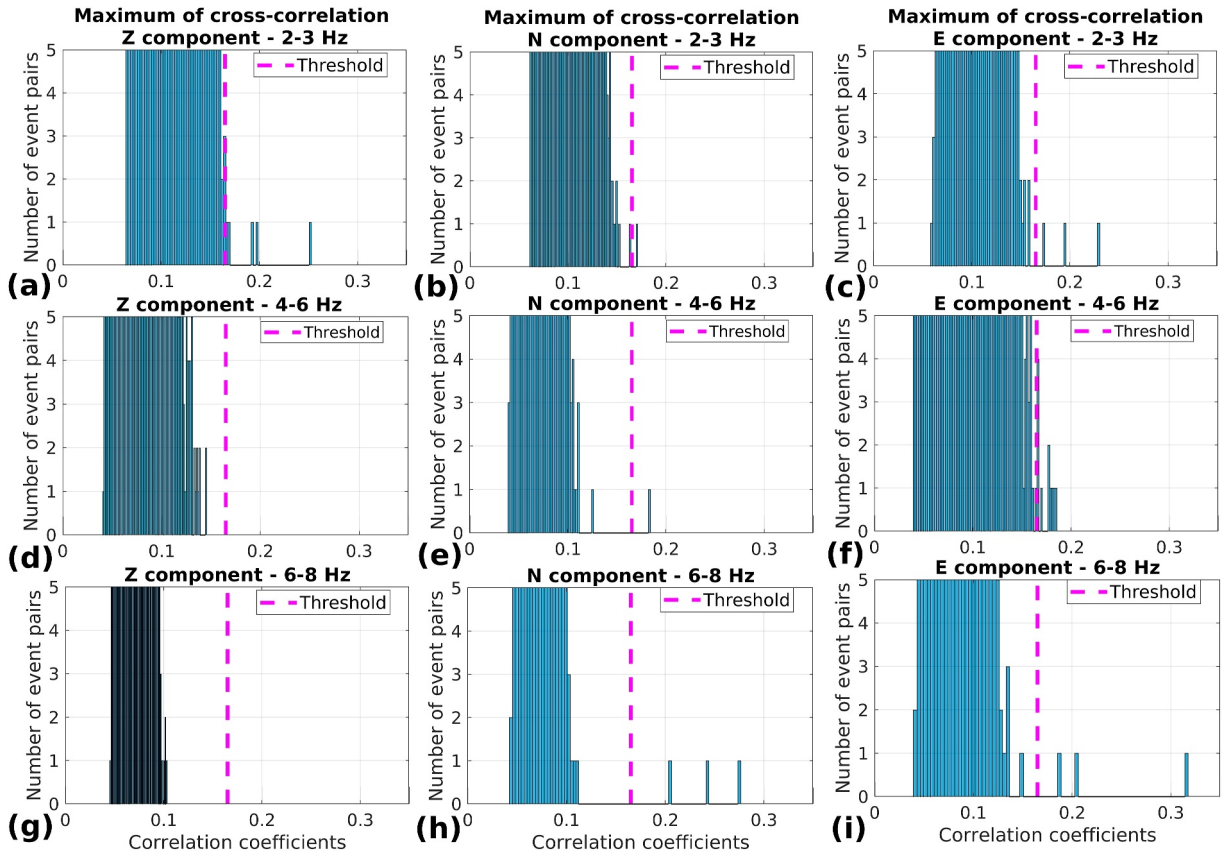

Figure 2. Distribution of Maximum Absolute Values of the Correlation Functions (MAVCF) for the 1,226 InSight seismic events, filtered in the 2–3 Hz (a, b, and c), the 4–6 Hz (d, e, and f) and the 6–8 Hz (g, h, and i) frequency bands, for the vertical (a, d, and g), North (b, e, and h) and East (c, f, and i) components. The magenta dashed line shows the doublet detection threshold at MAVCF = 0.17.

- The doublet candidate is detected on at least 2 components in the same frequency range. The doublet waveform is expected to be identical on the three components. However noise conditions and local site effect amplifications are different on the three components, thus impacting strongly the Signal-to-Noise-Ratio (SNR). For example, the vertical component shows a low SNR above 6 Hz and a high SNR at 2.4 Hz compared to the horizontal components.
- The MAVCF of the filtered records is larger without 1 bit normalization than with this 1 bit normalization. This is also expected for doublet repeating waveforms above the noise.
- All the time shifts obtained (with and without 1 bit normalization, and on all components for which there is a detection) are within 0.4 s. The quake doublet waveforms should be identical over all components and frequencies thus providing the exact same time shift. However, as the frequency bandwidths are relatively narrow in this analysis, we assumed that the peak of the correlation can be missed by half a period on both sides of a 2.4 Hz mode energy dominated signal.

Once these rules are applied only four doublets remain, detailed in Table 1.

3.3. Detailed Analysis of the Impact of Signal-To-Noise on the Correlation Properties

In order to fully validate a doublet candidate, we perform a final synthetic test aimed at demonstrating that the observed maximum correlation coefficients are consistent with the signal-to-noise ratio of the events. This test assumes that the record of the highest signal-to-noise event (event 1) in the couple is the seismic signal of the doublet. Then, a synthetic record of the second event is created by scaling the first event to the amplitude of the second event, and adding the noise recorded before the second event multiplied by a constant scaling factor. A synthetic record of the first event is then created by adding the noise recorded before the first event multiplied by a constant scaling factor to the waveform. The scaling factors are chosen to reproduce roughly the curves of signal-

Table 1
Summary of the Event Doublet Candidates Detected by Using the 0.17 Threshold on MAVCF Values on 1 Bit Normalized Waveforms for Different Components and Different Frequency Bands

First event and type	Second event and type	Components at 2–3 Hz MAVCF values (1-bit, non 1-bit)	Components at 4–6 Hz MAVCF values (1-bit, non 1-bit)	Components at 6–8 Hz MAVCF values (1-bit, non 1-bit)	Time shift (s)
S1008a	S1073d	Z (0.197,0.254)	none	none	3.45
HF	HF	E (0.195,0.254)			
S0343a	S0334b	Z (0.253,0.422)	E (0.185,0.305)	E (0.317,0.527)	40.85
VF	VF	E (0.229,0.398)		N (0.276,0.511)	
S0334c	S0334b	Z (0.194,0.344)	N (0.184,0.304)	E (0.205,0.378)	−136.6
VF	VF	E (0.172,0.330)		N (0.243,0.452)	
S0343a	S0334c	none	none	E (0.185,0.367)	177.45
VF	VF			N (0.204,0.408)	

Note. The MAVCF values are indicated in parenthesis with and without one bit normalization (1-bit, non 1-bit). The corresponding time shift between waveforms is indicated in the last column.

to-noise ratio which are computed by dividing the signal standard deviation estimated over moving 10 s windows with the noise standard deviation estimated over a 10 s window before the start of the event. Then, the MAVCF and the curves of correlation coefficients estimated over 10 s moving windows on the records aligned on their MAVCF are compared between the data and synthetic records.

The results of this validation test are presented for event pair S1073d/S1008a in Figure 3. The synthetic test predicts an MAVCF value of 0.488, whereas the InSight data present a value of only 0.254. As observed in panel (b) of Figure 3, this is mainly due to a decrease of the correlation properties in the S wave coda and partly also in the P wave coda. This feature could be explained by either an increased noise level during these time periods for the lowest signal-to-noise ratio event (S1008a), a possible overlap of the end of S1073d event with another event

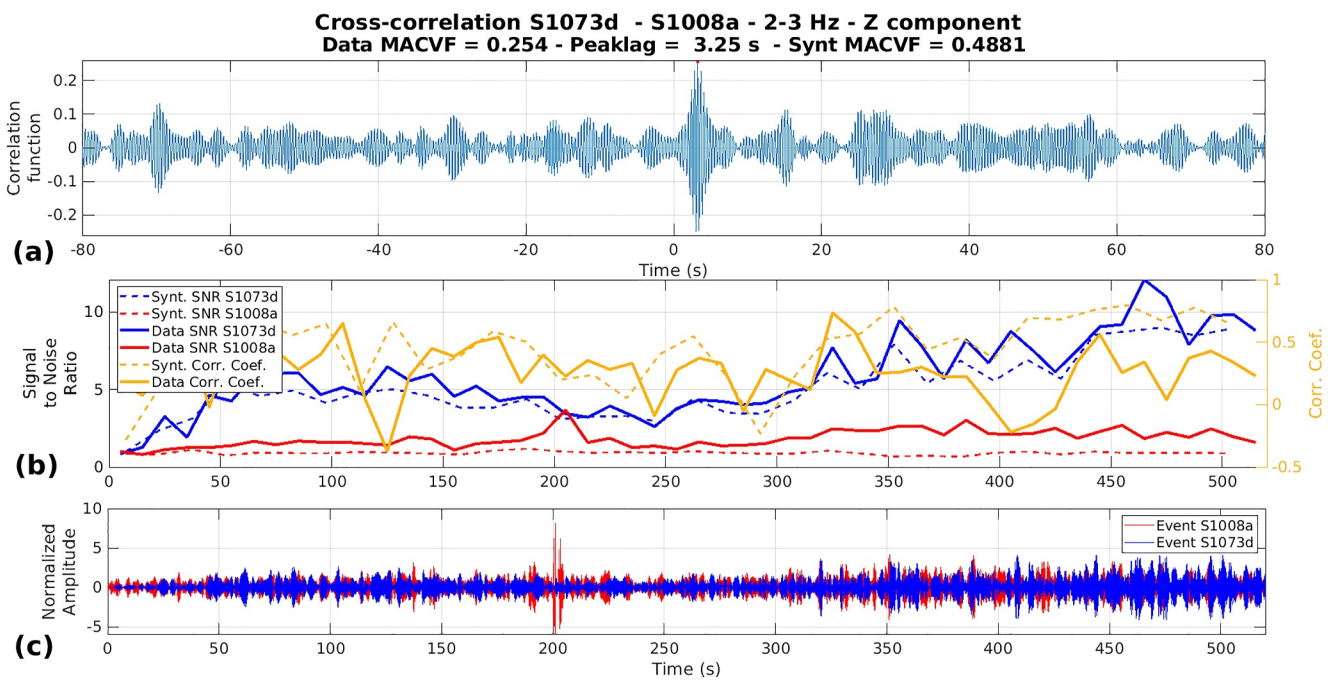

Figure 3. Correlation properties of doublet S1073d/S1008a in the 2–3 Hz range for the vertical (Z) component. (a) Correlation function of the two events. (b) Signal-to-noise ratio of S1073d (blue) and S1008a (red) and Correlation coefficient (gold) over 10 s windows for data (thick lines) and synthetic test (dashed lines). (c) Waveform of S1073d (blue) and S1008a (red) events after alignment on the maximum of the correlation function. The MAVCF values of data and synthetic test are indicated in the title of panel (a).

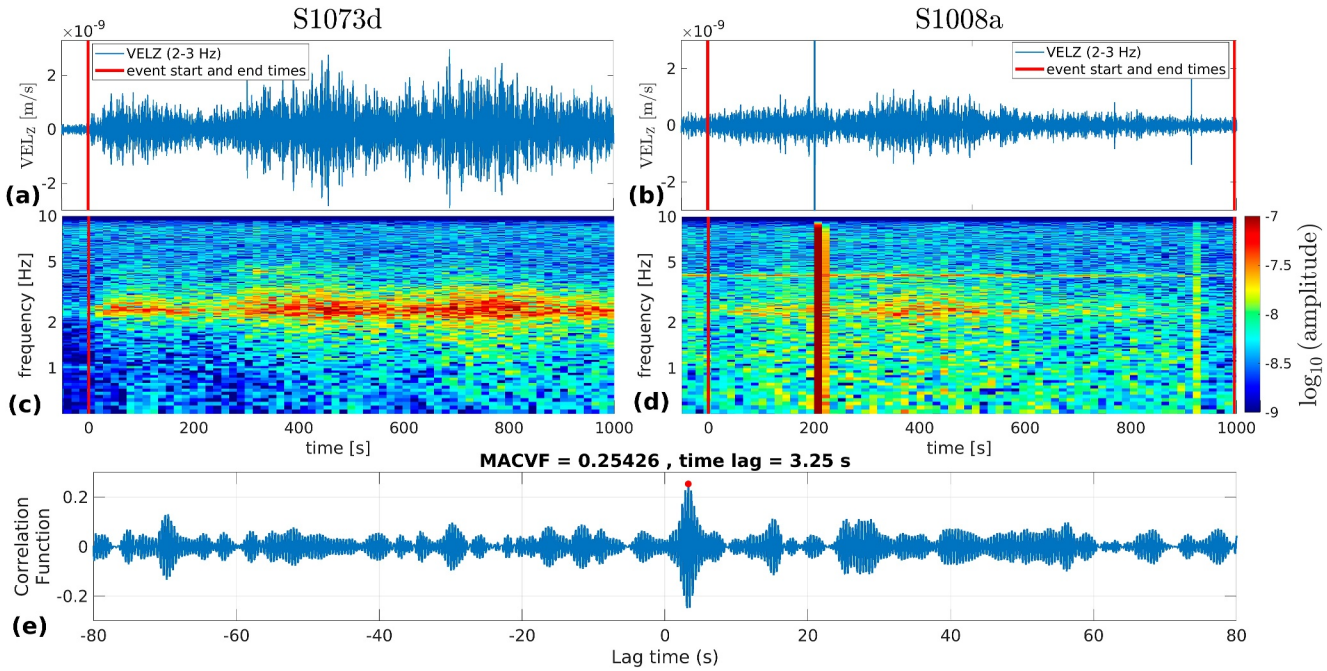

Figure 4. (a, b) Vertical component records filtered in the 2–3 Hz bandwidth and (c, d) their spectrograms, for events S1073d (left) and S1008a (right). Times are relative to MQS event start time (vertical red line). (e) Correlation function of the two records, Maximum Absolute Value (MAVCF) is indicated by a red dot. The artifact at 200 s on S1008a records is reduced by saturating the values at ±4 standard deviations of the records before computing the correlation function. Note the additional energy arriving after the first 500 s of event S1073d which is suggesting an overlap of this event with another one arriving after. The 4 Hz mode excitation observed on panel (b) is due to lander vibrations under the wind, suggesting that the lower signal-to-noise of event S1008a is due to wind noise contamination.

(see Figure 4 and Figure S1 in Supporting Information S1), or by a difference in event locations larger than a quarter wavelength that would not ensure identically scattered waves at InSight's location. The synthetic test demonstrates that event pair S1073d/S1008a cannot be straightforwardly validated as a doublet.

The results of the validation test are presented for the event doublet S0343a/S0334b in Figure 5. Only the highest signal-to-noise ratio waveforms are shown in this figure (vertical component in the 2–3 Hz range, and East component in the 6–8 Hz range) but similar results are obtained for the other components and in other frequency ranges (See Figure 6, Figures S2 and S3 in Supporting Information S1). For this doublet, the MAVCF values for data are comparable or larger than the ones obtained for the synthetic test. In addition, the correlation properties observed in panels (b) and (e) in Figure 5 closely follow the signal-to-noise ratio curves of the events and indicate that particularly high correlation is observed late in the S coda. This property is in good agreement with the interpretation of seismic events located on the exact same fault. As a consequence, we validate the S0343a/S0334b doublet as repeating seismic events occurring on the same fault.

Similar results are obtained for the doublet and S0334b/S0334c (See Figure 7, Figures S4 and S5 in Supporting Information S1) even if the MAVCF values are lower for the low signal-to-noise ratio of the S0334c event. These results support a triplet of repeating events on the same fault.

In addition, the low MAVCF values obtained for these pair of events in the vertical component in the 6–8 Hz range (see Figures S6–S8 and S15–S17 in Supporting Information S1) demonstrate that these signals are not due to atmospheric forcing that would also generate signals along the vertical component, but rather to seismic forcing that amplifies the signals above the noise in the horizontal components (Carrasco et al., 2023).

3.4. Potential Impact of Atmospheric Noise

We described in previous sections the potential impact of random noise on our results. However, the noise features in the InSight data are not random because they are mainly due to atmospheric forcing (Charalambous et al., 2021; Lognonné et al., 2020; Stott et al., 2023). As observed by various studies, the wind patterns on Mars can repeat with a given periodicity (Lorenz, 2022; Stott et al., 2025). However, the observed repeating features are

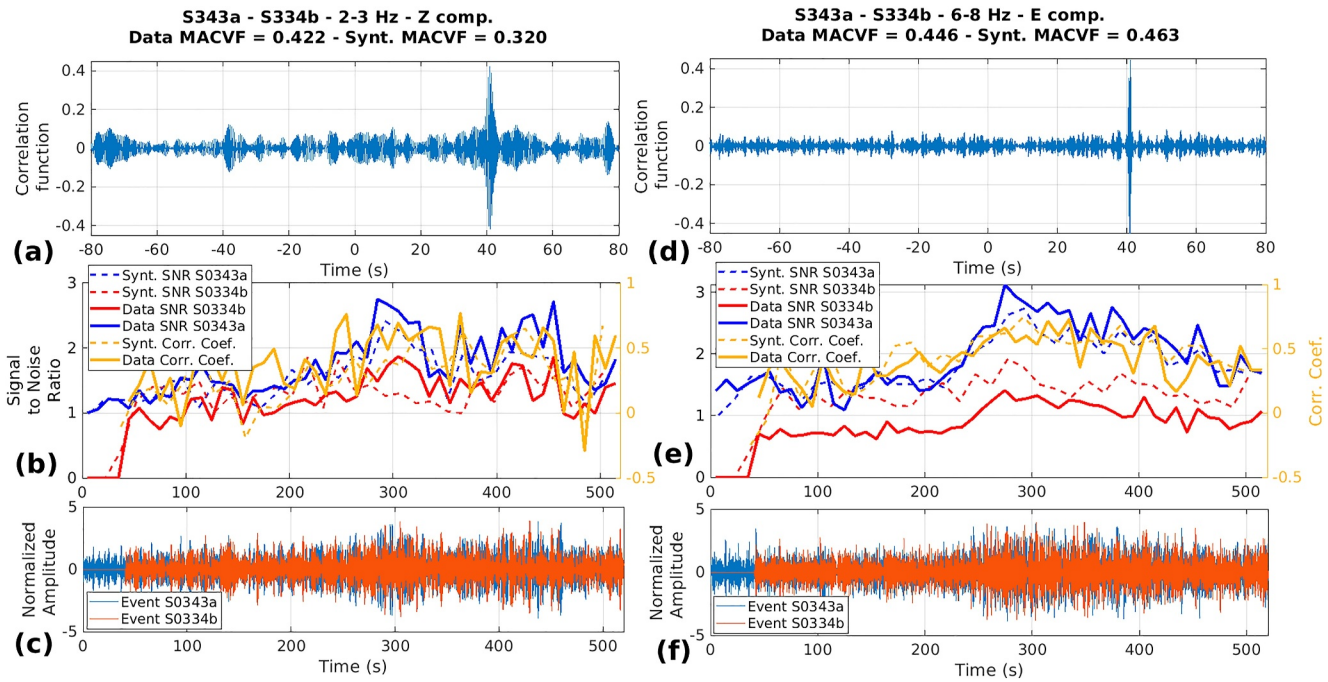

Figure 5. Correlation properties of doublet S0343a/S0334b in the 2–3 Hz range for the vertical (Z) component (a–c) and in the 6–8 Hz for the East (E) component (d–f). (a and d) Correlation function of the two events. (b and f) Signal-to-noise ratio of S0343a (blue) and S0334b (red) and Correlation coefficient (gold) over 10 s windows for data (thick lines) and synthetic test (dashed lines). (c and e) Waveforms of S0343a (blue) and S0334b (red) events after alignment on the maximum of the correlation function. The MAVCF values of data and synthetic test are indicated in the title of panels (a and c). Reference (zero) time is set 20 s before the P wave arrival provided by MQS. S wave arrival is estimated in the time range 222–250 s on these plots.

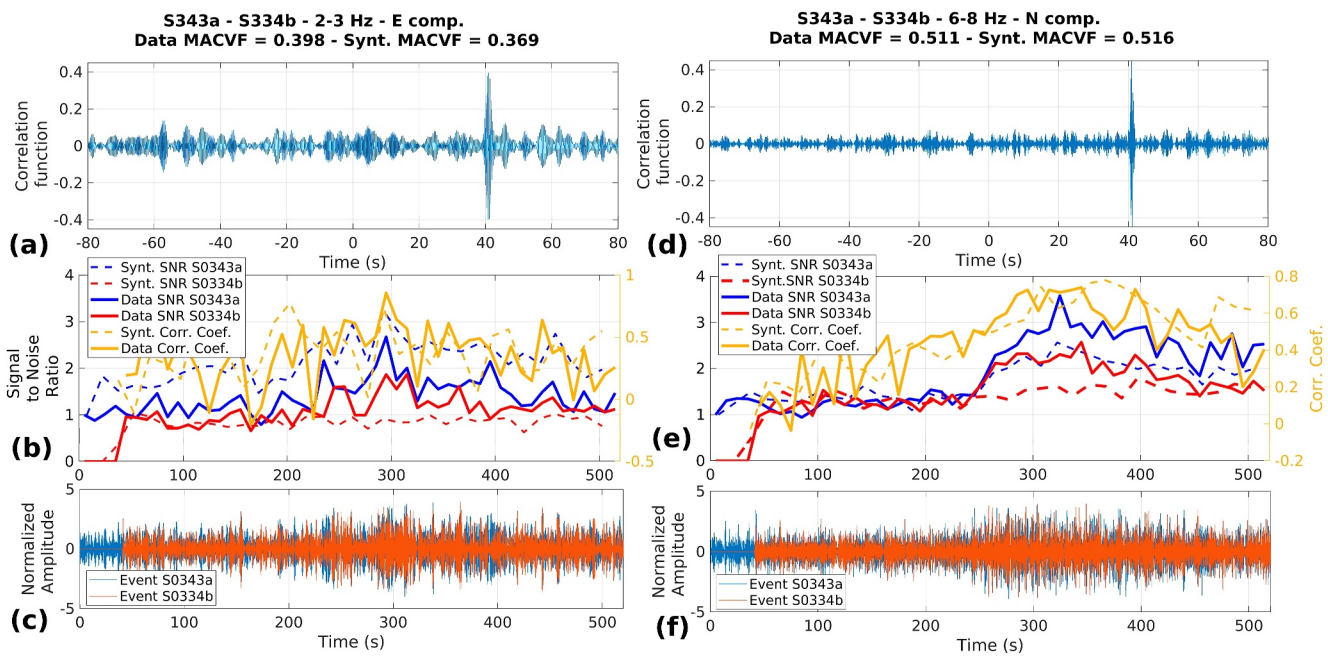

Figure 6. Correlation properties of doublet S0343a/S0334b in the 2–3 Hz range for the East (E) component (a–c) and in the 6–8 Hz for the North (N) component (d–f). (a and d) Correlation function of the two events. (b and f) Signal-to-noise ratio of S0343a (blue) and S0334b (red) and Correlation coefficient (gold) over 10 s windows for data (thick lines) and synthetic test (dashed lines). (c and e) Waveforms of S0343a (blue) and S0334b (red) events after alignment on the maximum of the correlation function. The MAVCF values of data and synthetic test are indicated in the title of panels (a and c). Reference (zero) time is set 20 s before the P wave arrival provided by MQS. S wave arrival is estimated in the time range 222–250 s on these plots.

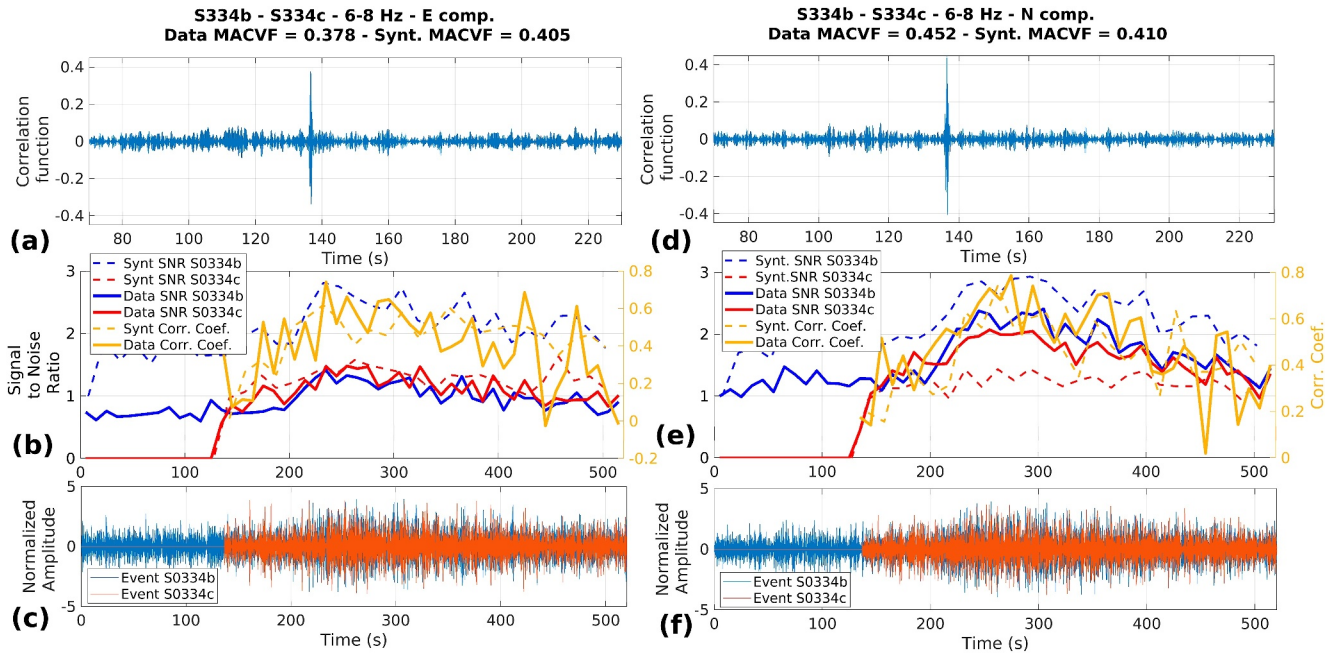

Figure 7. Correlation properties of doublet S0334b/S0334c in the 6–8 Hz range for the East (E) component (a–c) and for the North (N) component (d–f). (a and d) Correlation function of the two events. (b and f) Signal-to-noise ratio of S0334b (blue) and S0334c (red) and Correlation coefficient (gold) over 10 s windows for data (thick lines) and synthetic test (dashed lines). (c and e) Waveforms of S0334b (blue) and S0334c (red) events after alignment on the maximum of the correlation function. The MAVCF values of data and synthetic test are indicated in the title of panels (a and c). Reference (zero) time is set 20 s before the P wave arrival provided by MQS. S wave arrival is estimated in the time range 182–210 s on these plots.

related to the wind energy injected into the records of the seismometer. Most of the wind induced ground deformations are due to the response of the lander to wind forcing. This response induces lander vibration modes and a complex linear transfer function outside of the mode frequencies. However, this response remains linear and should maintain the wind forcing phase. Due to its intrinsically turbulent character, we consider that the wind effects cannot repeat with the same phase at frequencies above 2 Hz over the long durations considered here (>100 s). Since our method mainly uses the phase of the signal, we exclude wind variations as a potential source of contamination of our results.

In addition, these repeating wind patterns were only observed during daytimes (Lorenz, 2022; Stott et al., 2025) whereas our doublets are detected during the low wind nighttime periods of the martian day. Moreover, the excitation of the vertical component in the 6–8 Hz range expected for wind forcing is not observed for the candidate doublets (see Figures S6–S8, and S15–S17 in Supporting Information S1).

Overall, this sum of arguments allows us to exclude atmospheric forcing as the source of our doublet waveforms.

3.5. The S0343a/S0334b/S0334c Triplet of VF Type Events

The three VF type events show different SNRs, with the S0334c event having the lowest quality. The time shifts between the different records are consistent. As the S-P times determined by MQS are different for S0343a (223 s) and for S0334b (184 s) we decided to re-evaluate the S-P time of the S0343a waveform by picking the start of the P and S energy packets manually. The P wave pick is estimated 40 s later than the value provided by MQS, and the S wave pick in the time range 162–190 s after this P-wave pick. These arrivals are respectively at times 60 s and in the range 222–250 s in Figures 5 and 6. Due to a larger bandwidth for the seismic energy of these VF events, a reanalysis of the correlations can be performed in the 2–8 Hz range. When expanding the bandwidth of the data, a single positive correlation peak appears and the correlation function is symmetric around this maximum value (see panels (c) and (d) of Figure 8) for both pairs of events. This observation indicates that the three events have the same polarity, and so the same fault with a movement in the same direction.

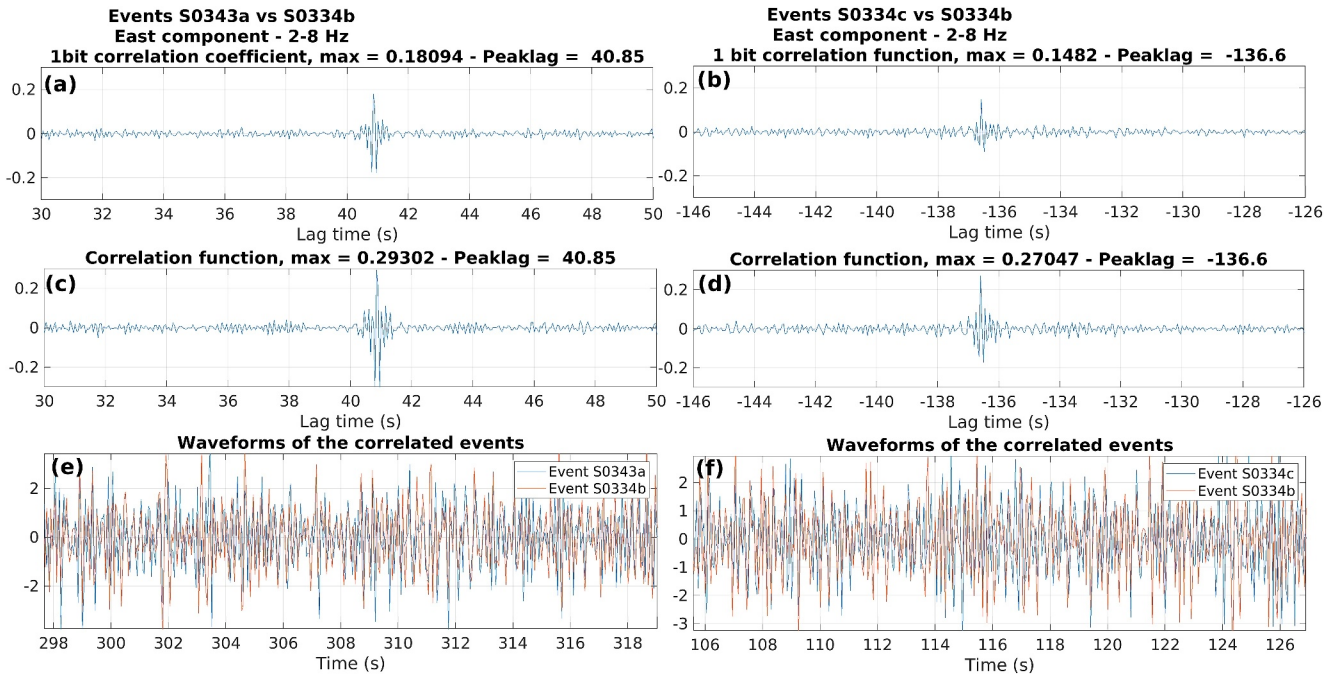

Figure 8. Example of correlation analysis for East component records of events doublets S0343a/S0334b (on the left, panels a, c, e) and S0334c/S0334b (on the right, panels b, d, f) in the 2–8 Hz frequency range. For each doublet, the correlation function of the 1 bit signals (a, b) and records without 1 bit normalization (c, d) as well as filtered records in time domain after alignment on highest correlation (e, f) are shown. Time domain records are normalized to their standard deviation to allow for a better comparison. The maximum value and corresponding time shift of correlation functions are provided in the title of panels a–d. Reference (zero) time is set 20 s before the P wave arrival provided by MQS for the first event. The waveforms in panels (e, f) are corresponding to a time range 100 s after S wave arrival.

3.6. Comparison With Previous Studies

Only a few studies investigated repeating events in InSight data set. A first attempt was made by Ceylan et al. (2022) by comparing the coda shapes of various high-frequency events. Highly correlated coda shapes are expected for events at similar distances (Menina et al., 2023), but do not demonstrate that these events repeat on the same fault because the phase of the signal is not used.

Another attempt correlated 12 s of event waveforms centered on P and S wave arrivals in order to detect overlapping events (N. Dahmen et al., 2024). These overlapping events were called doublets. However, this analysis, which relies solely on a few seconds of direct wave arrivals, does not establish the equivalence of scattered wavefields between these overlapping events, and so that these events are repeating on the same fault as expected for doublets (Gao et al., 2021). These overlapping events are not detected by our analysis because we do not correlate one event with itself. In addition, our method would not work for such events waveforms that overlap because the coda of one event is masked by the signals of the other event.

N. Dahmen et al. (2024) also identified pairs of events as aftershocks. Regarding the event pair S0918a/S0918b, our method is not applicable because these events do not have energy above 1 Hz. Concerning event pairs S0235b/S0235c and S0235b/S0235e, Figures S9 and S10 in Supporting Information S1 demonstrate that they are not doublets because their MAVCF values around 2.4 Hz local resonance are well below our threshold criteria. These events may be aftershocks on different fault segments but not doublets occurring on the same fault segment.

N. Dahmen et al. (2024) also identified a sequence of events related to the event 1157a that are potential aftershocks. Figures S11 and S12 in Supporting Information S1 demonstrate that event pairs S1157a/S1157f and S1157a/S1157g are not doublets that occur on the same fault segment, without excluding potential aftershocks that occur on different fault segments.

Eventually, due to similar S-P times and events that occur during the same sol, the event pairs S0334a/S0334b and S0334a/S0334c may be considered as doublets. Figures S13 and S14 in Supporting Information S1 demonstrate that it is not the case despite the high SNR values for event S0334a.

4. Discussion

Despite only a single multiplet detected in the InSight data, these events provide unique constraints on Mars seismic signals and seismicity.

First, the validation of these events as repeating quakes implies that the seismic vibrations should be identical but recorded under different noise conditions. As a consequence, these events can be used to test the efficiency of noise removal methods (Barkaoui et al., 2021; N. L. Dahmen et al., 2022; Scholz et al., 2020; Stott et al., 2023; Xu et al., 2022). Such methods should increase the waveform correlation between events after their application.

Furthermore, detection of the VF event triplet both at 2.4 Hz and in the 4–8 Hz frequency range demonstrates that the signal at 2.4 Hz recorded during seismic events is created by ground motion and contains some seismic information. This argument thus suggests again that the variation of energy in the 2.4 Hz resonance is a marker of the background seismic noise of Mars, as already suggested by noise auto-correlation studies (Compaire et al., 2021). However, our observations do not allow us to decipher between a sub-surface resonance (Hobiger et al., 2021), and a resonance in the InSight landing system (Pike et al., 2024).

In addition, these doublet events must be quakes occurring on the same fault and thus demonstrate that the VF type events contain both impacts (Charalambous et al., 2025; Garcia et al., 2022) and quakes. This result is in contradiction with the interpretation of all VF events being impacts suggested by Zenhäusern et al. (2024). However, if no seismically active areas are present at distances shorter than 25° because Cerberus area is the closest active seismic region, it remains possible that all VF events with S-P time below 165 s are all generated by impacts. This is not due to the event type (VF, HF or 2.4 Hz) but more to the absence of quakes in this region close to InSight. For this interpretation, we use the internal Mars structure models of Drilleau et al. (2022), seismic events at the surface, and interpret Pg and Sg picks provided by MQS as P and S waves propagating through the mantle as in Charalambous et al. (2025).

In addition, because the time separation between the doublet events is smaller than 10 sols, and could be smaller than 1 hr for S0334b/S0334c, these quakes are certainly associated to a sequence of seismic or volcanic activity. The epicentral distance provided by the S-P time of the VF triplet is consistent with a location in Cerberus Fossae.

Due to the strong impact of the low signal-to-noise ratio of the events detected by InSight, we cannot exclude that other event doublets are still hidden in the InSight data set. As a consequence, it is difficult to compare the statistics of doublets on Mars with those for the Earth or the Moon. However, the small and variable time separation between the VF events belonging to the VF triplet suggests an active seismic or volcanic sequence is the cause as is observed on the Earth (Uchida & Bürgmann, 2019). In contrast, repeating events on the Moon are driven by tidal stresses and repeat continuously at regular separation times (Nakamura, 2005; Weber et al., 2009).

5. Conclusions

The quake nests detection method presented here has been validated and applied to the InSight SEIS data. A clear triplet of VF events repeating with the same polarity is detected and validated through a synthetic test of the impact of the noise on our method. A potential doublet of HF events is excluded due to the contamination by noise sources or by an overlap with another event. Despite the small number of quake doublets detected, likely due to the low signal-to-noise ratio of the vast majority of marsquakes, our study demonstrates that repeating quakes do occur on Mars, as they do on Earth and the Moon. These events could be used to test noise removal methods and validate a seismic active zone at ∼26° distance (S-P times of ∼180 s). In addition, the VF triplet confirms the seismic character of the 2.4 Hz resonance (Compaire et al., 2021), and thus suggests again that energy variations observed at this frequency during the early night time could be due to background seismic noise variations.

Because their S-P differential times are comparable with those of LF events located (through back azimuths) in the vicinity of Cerberus Fossae, the VF event triplet can be associated with the seismicity of this region. Thus the VF event category has now been shown to include both quakes (this study) and impacts (Charalambous et al., 2025; Daubar et al., 2023; Garcia et al., 2022). As a consequence, not all VF events are impacts as recently suggested (Zenhäusern et al., 2024).

Data Availability Statement

Data processing performed in this study was done with standard MATLAB functions. InSight's SEIS data are available at IRIS-DMC and PDS in the SEED format (InSight Mars SEIS Data Service, 2019). The marsquake event catalog version 14 (InSight Marsquake Service, 2023) produced by Mars Quake Service is used in this study.

Acknowledgments
The authors acknowledge there are no conflicts of interest recorded. The authors thanks Vedran Lekic for suggesting the time reversal statistical evaluation method of MAVCF. This study is InSight contribution number 334. The French authors acknowledge the French Space Agency CNES and ANR (ANR-14-CE36-0012-02 and ANR-19-CE31-0008-08) for funding the InSight Science analysis. We acknowledge NASA, CNES, their partner agencies and institutions (UKSA, SSO, DLR, JPL, IPGP-CNRS, ETHZ, IC, and MPS-MPG), and the flight operations team at JPL, SISMOC, MSDS, IRIS-DMC, and PDS for providing SEED SEIS data. SEIS data are referenced at http://dx.doi.org/10.18715/SEIS.INSIGHT.XB_2016.

References

Banerdt, W. B., Smrekar, S. E., Banfield, D., Giardini, D., Golombek, M., Johnson, C. L., et al. (2020). Initial results from the InSight mission on Mars. *Nature Geoscience*, *13*(3), 1–14. https://doi.org/10.1038/s41561-020-0544-y

Barkaoui, S., Lognonné, P., Kawamura, T., Stutzmann, É., Seydoux, L., de Hoop, M. V., et al. (2021). Anatomy of continuous Mars SEIS and pressure data from unsupervised learning. *Bulletin of the Seismological Society of America*, *111*(6), 2964–2981. https://doi.org/10.1785/0120210095

Carrasco, S., Knapmeyer-Endrun, B., Margerin, L., Schmelzbach, C., Onodera, K., Pan, L., et al. (2023). Empirical H/V spectral ratios at the InSight landing site and implications for the Martian subsurface structure. *Geophysical Journal International*, *232*(2), 1293–1310. https://doi.org/10.1093/gji/ggac391

Ceylan, S., Clinton, J. F., Giardini, D., Stähler, S. C., Horleston, A., Kawamura, T., et al. (2022). The marsquake catalogue from InSight, sols 0–1011. *Physics of the Earth and Planetary Interiors*, *333*, 106943. https://doi.org/10.1016/j.pepi.2022.106943

Charalambous, C., Pike, W. T., Fernando, B., Wójcicka, N., Kim, D., Froment, M., et al. (2025). New impacts on Mars: Unraveling seismic propagation paths through a Cerberus Fossae impact detection. *Geophysical Research Letters*, *52*(3), 2024GL110159. https://doi.org/10.1029/2024GL110159

Charalambous, C., Stott, A. E., Pike, W. T., McClean, J. B., Warren, T., Spiga, A., et al. (2021). A comodulation analysis of atmospheric energy injection into the ground motion at InSight, Mars. *Journal of Geophysical Research (Planets)*, *126*(4), e06538. https://doi.org/10.1029/2020JE006538

Clinton, J. F., Ceylan, S., van Driel, M., Giardini, D., Stähler, S. C., Böse, M., et al. (2021). The marsquake catalogue from InSight, sols 0–478. *Physics of the Earth and Planetary Interiors*, *310*, 106595. https://doi.org/10.1016/j.pepi.2020.106595

Compaire, N., Margerin, L., Garcia, R. F., Pinot, B., Calvet, M., Orhand-Mainsant, G., et al. (2021). Autocorrelation of the ground vibrations recorded by the SEIS InSight seismometer on Mars. *Journal of Geophysical Research (Planets)*, *126*(4), e06498. https://doi.org/10.1029/2020JE006498

Dahmen, N., Clinton, J., Stähler, S., Meier, M.-A., Ceylan, S., Euchner, F., et al. (2024). Revisiting Martian seismicity with deep learning-based denoising. *Geophysical Journal International*, *239*(1), 434–454. https://doi.org/10.1093/gji/ggae279

Dahmen, N. L., Clinton, J. F., Meier, M.-A., Stähler, S. C., Ceylan, S., Kim, D., et al. (2022). MarsQuakeNet: A more complete marsquake catalog obtained by deep learning techniques. *Journal of Geophysical Research (Planets)*, *127*(11), e2022JE007503. https://doi.org/10.1029/2022JE007503

Daubar, I. J., Fernando, B. A., Garcia, R. F., Grindrod, P. M., Zenhäusern, G., Wójcicka, N., et al. (2023). Two seismic events from InSight confirmed as new impacts on Mars. *Planetary Science Journal*, *4*(9), 175. https://doi.org/10.3847/PSJ/ace9b4

Drilleau, M., Beucler, É., Shi, J., Knapmeyer-Endrun, B., Garcia, R. F., Ansan, V., et al. (2023). Structure of the Martian crust below InSight from surface waves and body waves generated by nearby Meteoroid impacts. *Geophysical Research Letters*, *50*(23), e2023GL104601. https://doi.org/10.1029/2023GL104601

Drilleau, M., Samuel, H., Garcia, R. F., Rivoldini, A., Perrin, C., Michaut, C., et al. (2022). Marsquake locations and 1-D seismic models for Mars from InSight data. *Journal of Geophysical Research (Planets)*, *127*(9), e07067. https://doi.org/10.1029/2021JE007067

Frohlich, C., & Nakamura, Y. (2009). The physical mechanisms of deep moonquakes and intermediate-depth earthquakes: How similar and how different? *Physics of the Earth and Planetary Interiors*, *173*(3–4), 365–374. https://doi.org/10.1016/j.pepi.2009.02.004

Gao, D., Kao, H., & Wang, B. (2021). Misconception of waveform similarity in the identification of repeating earthquakes. *Geophysical Research Letters*, *48*(13), e92815. https://doi.org/10.1029/2021GL092815

Garcia, R. F., Daubar, I. J., Beucler, É., Posiolova, L. V., Collins, G. S., Lognonné, P., et al. (2022). Newly formed craters on Mars located using seismic and acoustic wave data from insight. *Nature Geoscience*, *15*(10), 774–780. https://doi.org/10.1038/s41561-022-01014-0

Giardini, D., Lognonné, P., Banerdt, W. B., Pike, W. T., Christensen, U., Ceylan, S., et al. (2020). The seismicity of Mars. *Nature Geoscience*, *13*(3), 205–212. https://doi.org/10.1038/s41561-020-0539-8

Hobiger, M., Hallo, M., Schmelzbach, C., Stähler, S. C., Fäh, D., Giardini, D., et al. (2021). The shallow structure of Mars at the InSight landing site from inversion of ambient vibrations. *Nature Communications*, *12*(1), 6756. https://doi.org/10.1038/s41467-021-26957-7

InSight Marsquake Service. (2023). Mars seismic catalogue, insight mission; v14 2023-04-01 [Dataset]. *ETHZ, IPGP, JPL, ICL, Univ. Bristol*. https://doi.org/10.12686/a21

InSight Mars SEIS Data Service. (2019). Seis raw data [Dataset]. *Insight Mission*. https://doi.org/10.18715/SEIS.INSIGHT.XB_2016

Jacob, A., Plasman, M., Perrin, C., Fuji, N., Lognonné, P., Xu, Z., et al. (2022). Seismic sources of insight marsquakes and seismotectonic context of Elysium Planitia, Mars. *Tectonophysics*, *837*, 229434. https://doi.org/10.1016/j.tecto.2022.229434

Lammlein, D. R. (1977). Lunar seismicity and tectonics. *Physics of the Earth and Planetary Interiors*, *14*(3), 224–273. https://doi.org/10.1016/0031-9201(77)90175-3

Lognonné, P., Banerdt, W. B., Giardini, D., Pike, W. T., Christensen, U., Laudet, P., et al. (2019). SEIS: Insight's seismic experiment for internal structure of Mars. *Space Science Reviews*, *215*(1), 12. https://doi.org/10.1007/s11214-018-0574-6

Lognonné, P., Banerdt, W. B., Pike, W. T., Giardini, D., Christensen, U., Garcia, R. F., et al. (2020). Constraints on the shallow elastic and Anelastic structure of Mars from InSight seismic data. *Nature Geoscience*, *13*(3), 213–220. https://doi.org/10.1038/s41561-020-0536-y

Lorenz, R. D. (2022). Wait a minute Martian wind autocorrelations. In F. Forget & M. Millour (Eds.), *Seventh international workshop on the Mars atmosphere: Modelling and observations*, (p. 1518).

Margerin, L. (2013). Diffusion approximation with polarization and resonance effects for the modelling of seismic waves in strongly scattering small-scale media. *Geophysical Journal International*, *192*(1), 326–345. https://doi.org/10.1093/gji/ggs022

Menina, S., Margerin, L., Kawamura, T., Heller, G., Drilleau, M., Xu, Z., et al. (2023). Stratification of heterogeneity in the lithosphere of Mars from envelope modeling of event S1222a and near impacts: Interpretation and implications for very-high-frequency events. *Geophysical Research Letters*, *50*(7), e2023GL103202. https://doi.org/10.1029/2023GL103202

Menina, S., Margerin, L., Kawamura, T., Lognonné, P., Marti, J., Drilleau, M., et al. (2021). Energy envelope and attenuation characteristics of High-Frequency (HF) and Very-high-Frequency (VF) Martian events. *Bulletin of the Seismological Society of America*, *111*(6), 3016–3034. https://doi.org/10.1785/0120210127

Nakamura, Y. (1978). A moonquakes: Source distribution and focal mechanism. In *Lunar and planetary Science Conference* (pp. 796–798).

Nakamura, Y. (2005). Farside deep moonquakes and deep interior of the Moon. *Journal of Geophysical Research (Planets)*, *110*(E1), E01001. https://doi.org/10.1029/2004JE002332

Perrin, C., Jacob, A., Lucas, A., Myhill, R., Hauber, E., Batov, A., et al. (2022). Geometry and segmentation of Cerberus Fossae, Mars: Implications on marsquake properties in Elysium Planitia. *Journal of Geophysical ResearchEducational Planning*, *127*(1), e2021JE007118. https://doi.org/10.1029/2021JE007118

Pike, W. T., Charalambous, C., Fernando, B., Lognonne, P., & Panning, M. (2024). The effect of Regolith properties in coupling Lander resonances to the seismic and atmospheric signals of SEIS. *Mars Interior and Geophysics After Insight*, *3060*, 6062.

Posiolova, L., Lognonné, P., Banerdt, W. B., Clinton, J., Collins, G. S., Kawamura, T., et al. (2022). Largest recent impact craters on Mars: Orbital imagery and surface seismic co-investigation. *Science*, *378*(6618), 412–417. https://doi.org/10.1126/science.abq7704

Poupinet, G., Ellsworth, W. L., & Frechet, J. (1984). Monitoring velocity variations in the crust using earthquake doublets: An application to the Calaveras fault, California. *Journal of Geophysical Research*, *89*(B7), 5719–5731. https://doi.org/10.1029/JB089iB07p05719

Scholz, J.-R., Widmer-Schnidrig, R., Davis, P., Lognonné, P., Pinot, B., Garcia, R. F., et al. (2020). Detection, analysis, and removal of glitches from InSight's seismic data from Mars. *Earth and Space Science*, *7*(11), e01317. https://doi.org/10.1029/2020EA001317

Snieder, R. (2006). The theory of coda wave interferometry. *Pure and Applied Geophysics*, *163*(2–3), 455–473. https://doi.org/10.1007/s00024-005-0026-6

Stähler, S. C., Mittelholz, A., Perrin, C., Kawamura, T., Kim, D., Knapmeyer, M., et al. (2022). Tectonics of Cerberus fossae unveiled by marsquakes. *Nature Astronomy*, *6*(12), 1376–1386. https://doi.org/10.1038/s41550-022-01803-y

Stott, A. E., Garcia, R. F., Chédozeau, A., Spiga, A., Murdoch, N., Pinot, B., et al. (2023). Machine learning and marsquakes: A tool to predict atmospheric-seismic noise for the NASA InSight mission. *Geophysical Journal International*, *233*(2), 978–998. https://doi.org/10.1093/gji/ggac464

Stott, A. E., Garcia, R. F., Murdoch, N., Mimoun, D., Drilleau, M., Newman, C., et al. (2025). WindSightNet: The inter-annual variability of Martian winds retrieved from InSight's seismic data with machine learning. *Journal of Geophysical Research (Planets)*, *130*(2), 2024JE008695. https://doi.org/10.1029/2024JE008695

Uchida, N., & Bürgmann, R. (2019). Repeating earthquakes. *Annual Review of Earth and Planetary Sciences*, *47*(1), 305–332. https://doi.org/10.1146/annurev-earth-053018-060119

van Driel, M., Ceylan, S., Clinton, J. F., Giardini, D., Horleston, A., Margerin, L., et al. (2021). High frequency seismic events on Mars observed by InSight. *Journal of Geophysical Research (Planets)*, *126*(2), e06670. https://doi.org/10.1029/2020JE006670

Weber, R. C., Bills, B. G., & Johnson, C. L. (2009). Constraints on deep moonquake focal mechanisms through analyses of tidal stress. *Journal of Geophysical Research (Planets)*, *114*(E5), E05001. https://doi.org/10.1029/2008JE003286

Xu, W., Zhu, Q., & Zhao, L. (2022). GlitchNet: A glitch detection and removal system for SEIS records based on deep learning. *Seismological Research Letters*, *93*(5), 2804–2817. https://doi.org/10.1785/0220210361

Zenhäusern, G., Wójcicka, N., Stähler, S. C., Collins, G. S., Daubar, I. J., Knapmeyer, M., et al. (2024). An estimate of the impact rate on Mars from statistics of very-high-frequency marsquakes. *Nature Astronomy*, *8*(9), 1138–1147. https://doi.org/10.1038/s41550-024-02301-z